Journal of Colloid and Interface Science 532 (2018) 598–604

Contents lists available at ScienceDirect

Journal of Colloid and Interface Science

journal homepage: www.elsevier.com/locate/jcis

Regular Article

The selectively fluorescent sensing detection and adsorptive removal of Pb^{2+} with a stable [δ-Mo_8O_{26}]-based hybrid

Xiao-Xu Song [a,b], Huifen Fu [a,b], Peng Wang [a,b], Hai-Yan Li [b], Yan-Qiu Zhang [c], Chong-Chen Wang [a,b,*]

[a] Beijing Key Laboratory of Functional Materials for Building Structure and Environment Remediation, Beijing University of Civil Engineering and Architecture, Beijing 100044, China
[b] Beijing Engineering Research Center of Sustainable Urban Sewage System Construction and Risk Control, Beijing University of Civil Engineering and Architecture, Beijing 100044, China
[c] State Key Laboratory of Pollution Control and Resource Reuse, College of Environmental Science & Engineering, Tongji University, Shanghai 200092, China

GRAPHICAL ABSTRACT

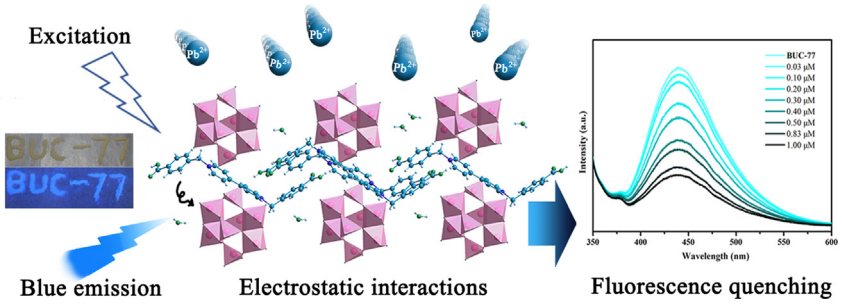

ARTICLE INFO

Article history:
Received 23 June 2018
Revised 2 August 2018
Accepted 9 August 2018
Available online 10 August 2018

Keywords:
Fluorescence
Adsorption
Polyoxomolybdate
Pb^{2+}
Selective detection

ABSTRACT

A polyoxomolybdate based hybrid, [δ-Mo_8O_{26}](L)$_2$·2H_2O (**BUC-77**), was synthesized via hydrothermal method, which exhibited selectively fluorescent detection and efficient adsorptive removal toward Pb^{2+} in aqueous environment. A good linearity was observed between the fluorescence quenching percentage of **BUC-77** and the Pb^{2+} concentration, along with the detection limit being 6.91 ppb. **BUC-77** was stable in common solvents and wide pH range, which could be regenerated by being washed with dilute inorganic acids like HNO_3 after adsorption of Pb^{2+}. The results revealed that **BUC-77** could be potentially used to achieve both detection and removal of Pb^{2+} in wastewater.

1. Introduction

Polyoxometalates (POMs) based organic-inorganic hybrid crystalline materials have attracted wide attention due to not only their versatile architectures, but also their excellent properties with promising applications [1] including but not limited to catalysis [2–4], adsorption [5–7], separation [8–10], anti-microbial [11], sensing for small molecules, medical diagnostics and cell biology [12–15]. As a representative member of POM, octamolybdates are good block to generate various hybrids with novel topologies. Up to now, eight isomeric octamolybdate forms like α, β, γ, δ, ε, ζ, η and θ isomers have been reported to construct hybrids with organic linkers and/or metal ions [16–18].

It is reported that (4-Hap)$_4$[β-Mo_8O_{26}] (4-ap = 4-aminopyridine) (**BUC-14**) exhibited excellent adsorption performance toward organic pollutants like methylene blue (MB) [19] and heavy metals like Pb^{2+} [20], which also demonstrated

* Corresponding author at: Beijing Key Laboratory of Functional Materials for Building Structure and Environment Remediation, Beijing University of Civil Engineering and Architecture, Beijing 100044, China.
E-mail address: wangchongchen@bucea.edu.cn (C.-C. Wang).

https://doi.org/10.1016/j.jcis.2018.08.029
0021-9797/

outstanding separation activities towards environmental pollutants with different charge [19,20]. Just recently, our group is paying more attention to prepare the multifunctional organic-inorganic hybrid crystalline materials with high adsorption capacity and fluorescent sensing property. In this study, [δ-Mo_8O_{26}](L)$_2$·2H_2O (**BUC-77**) was synthesized from 1,1′-bis(4-carboxylato benzyl)-4,4′-bipyridinium dichloride (L) and ammonium molybdate (as illustrated in Scheme S1). **BUC-77** could be used as selective fluorescence sensing toward Pb^{2+} ions. As well, it demonstrated efficient adsorptive performance toward Pb^{2+} ions from the simulated wastewater. The possible adsorption and sensing mechanisms were proposed, which were further affirmed by XPS, SEM-EDS and FTIR analyses.

2. Experimental

2.1. Materials and methods

All chemicals were commercially available reagent grade and used without further purification. Aqueous solutions of K^+, Na^+, Mg^{2+}, Ca^{2+}, Mn^{2+}, Ba^{2+}, Cu^{2+}, Zn^{2+}, Co^{2+}, Ni^{2+}, Pb^{2+}, Al^{3+} and Cd^{2+} were prepared from their corresponding chloride salts; Fe^{2+} solution was prepared from ferrous sulfate and used immediately.

CHN Elemental analyses were conducted on an Elementar Vario EL-III instrument. FTIR spectra were recorded on a Nicolet 6700 Fourier Transform infrared spectrophotometer ranging from 4000 to 400 cm^{-1}. The surface area of the sample was obtained by BELSORP-Mini II from N_2 adsorption – desorption isotherms at 77 K using Brunauer-Emmett-Teller nitrogen adsorption method (BET). Thermogravimetric analyses (TGA) were performed from 70 to 800 °C in an air stream at a heating rate of 10 °C/min on a DTU-3c thermal analyzer using α-Al_2O_3 as reference. UV–Vis diffuse reflectance spectra (DRS) of solid samples were measured from 200 nm to 800 nm on a PerkinElmer Lambda 650S spectrophotometer, in which barium sulfate ($BaSO_4$) was used as the standard with 100% reflectance. The surface charge of the particles was assessed by zeta potential measurements on the JS94H zeta sizer by applying the field strength of 10 V/cm. X-ray photoelectron spectra (XPS) measurement was conducted on a Thermo ESCALAB 250XI. Fluorescence spectra were recorded on a Hitachi F-7000 spectrophotometer at room temperature.

2.2. Synthesis of [δ-Mo_8O_{26}](L)$_2$·2H_2O (BUC-77)

A mixture of $ZnCl_2$ (0.3 mmol, 0.0408 g), 1,1′-bis(4-carboxylato benzyl)-4,4′-bipyridiniun)dichloride (L) (0.3 mmol, 0.1492 g) and ammonium molybdate tetrahydrate ($H_{24}Mo_7N_6O_{24}$·4H_2O, 0.3 mmol, 0.7415 g) with a molar ratio of 1:1:1 was sealed in a 25 mL Teflon-lined stainless steel Parr bomb containing deionized H_2O (20 mL), heated at 160 °C for 72 h, and then cooled down to room temperature. Light brown block-like crystals were isolated and washed with deionized water and ethanol (yield 87% based on $ZnCl_2$). Anal. Calcd. for **BUC-77**, $C_{52}H_{48}Mo_8N_4O_{36}$: C, 30.1; N, 2.7; H, 2.3. Found: C, 30.2; N, 2.7; H, 2.4. IR (KBr)/cm^{-1}: 3504, 1723, 1632, 1579, 1557, 1502, 1472, 1444, 1419, 1383, 1321, 1279, 1231, 1176, 1155, 1110, 1018, 931, 855, 798, 655, 552, 406.

2.3. Fluorescence sensing experiment

The suspension of fluorescent probe was prepared by dispersing 50 mg **BUC-77** powder with particle size less than 147 μm in 50 mL ultra-pure water via ultrasonic agitation for 30 min. Fluorescence responses of **BUC-77** toward aqueous solution containing various metals like K^+, Na^+, Mg^{2+}, Ca^{2+}, Mn^{2+}, Ba^{2+}, Cu^{2+}, Zn^{2+}, Co^{2+}, Ni^{2+}, Pb^{2+}, Al^{3+}, Fe^{2+} and Cd^{2+} cations were investigated. To further explore the possibility of **BUC-77** as fluorescent probe to detect Pb^{2+} ion, the fluorescence intensities of the matrix composed of series 3.0 mL as-prepared **BUC-77** suspensions and the aqueous solutions with different Pb^{2+} concentrations were determined after equilibrium for 20 min.

2.4. Adsorption experiments

25.0 mg **BUC-77** powders were added to 100 mL 10 mg/L Pb$(NO_3)_2$ aqueous solution in a 250 mL beaker (pH = 3.4). The suspensions were stirred for a desired time with an integrated thermostatic magnetic blender at a constant speed about 750 r/min under room temperature. 2.0 mL aliquot samples were extracted at fixed time intervals and separated using a 0.45 μm syringe filter (Shanghai Troody). The residual Pb^{2+} concentrations were analyzed by flame atomic absorption spectrophotometer (PinAAcle 900T).

3. Results and discussion

We failed to harvest **BUC-77** without the addition of $ZnCl_2$, implying $ZnCl_2$ might play a role of a catalyst and pH regulator [19,21]. **BUC-77** are stable and insoluble in water and common organic solvents, including but not limited to methanol, ethanol, ether and N,N-dimethylformamide (DMF).

3.1. Structural description of BUC-77

The structure of **BUC-77** was built up from of one discrete [δ-Mo_8O_{26}]$^{4-}$ anion and two cationic L^{2+} organic molecules. Each [δ-Mo_8O_{26}]$^{4-}$ anion, as shown in Fig. 1(a), is constructed from four [MoO_6] octahedra and four tetrahedral [MoO_4] via edge-sharing and corner-sharing arrangement. The Mo–O distances ranges from 1.686(4) to 2.380(4) Å resulted from the different interactions between cationic units and polyanionic units (Table S2). The structure of [δ-Mo_8O_{26}]$^{4-}$ anion in **BUC-77** is consistent with those reported counterparts [3,22–24], despite of slightly difference in Mo—O bond lengths. Each L^{2+} is joined to [δ-Mo_8O_{26}]$^{4-}$ to construct a 3D supramolecular framework via electrostatic interaction and hydrogen bonding interactions (O—H···O) (Table S3), which also acts as counter-ion to compensate the anionic charge of [Mo_8O_{26}]$^{4-}$ polyanions, as illustrated in Fig. 1(b).

3.2. Fluorescence properties of BUC-77

As illustrated in Fig. 2a, the free L molecule exhibited an intense fluorescent emission in aqueous solution at 526 nm (Fig. 2a), which can be assigned to the π^*–π transition of the free L. The **BUC-77** suspended in aqueous solution presented maximum emission peak at ca. 441 nm (λ_{ex} = 335 nm), which was significantly different from the peak at 526 nm of free L. The significant blue shift of the emission wavelength observed in **BUC-77** might be attributed to the ligand-to-metal charge transfer (LMCT)[25]. The fluorescence lifetime of **BUC-77** was determined to be τ =10 μs (Fig. S1), similar to the reported of other fluorescent counterparts [26,27].

The UV–Vis spectra (Fig. 2b) of **BUC-77** and discrete L were measured in the aqueous solution at room temperature in the region of 600–190 nm. The absorption peaks of 193, 229 and 256 nm corresponded to annular conjugate system transition and π-π^* transition absorption. The UV–Vis DRS spectra (Inset of Fig. 2b) of solid-state **BUC-77** and free L were analyzed at room temperature to investigate the interactions between the [Mo_8O_{26}]$^{4-}$ clusters and organic struts of L^{2+}. It is found that **BUC-77** exhibits an absorption band at 425 nm, quite different from the absorption of L at 520 nm, which can be assigned to the ligand-to-metal transition [28–30].

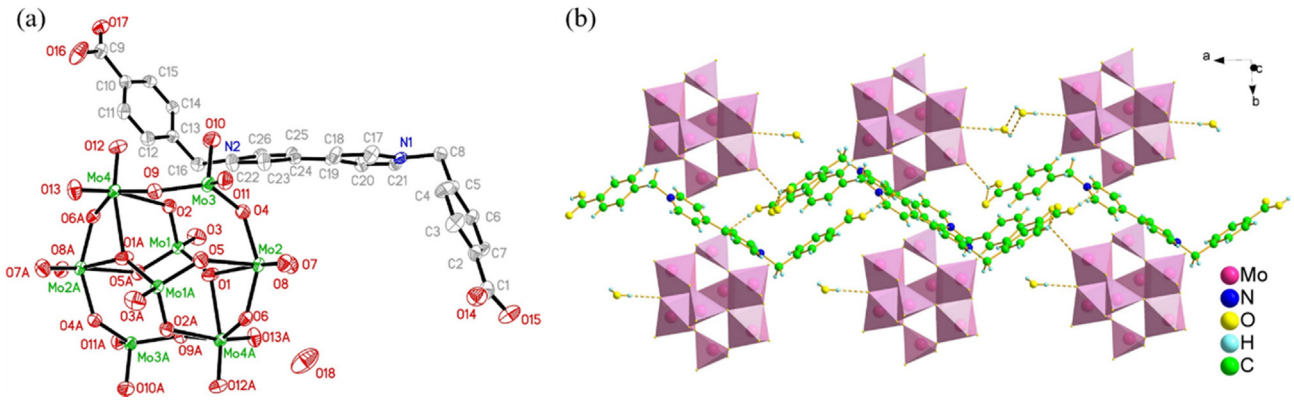

Fig. 1. (a) The asymmetric unit of **BUC-77**. (b) Detailed hydrogen-bonding interactions in **BUC-77**.

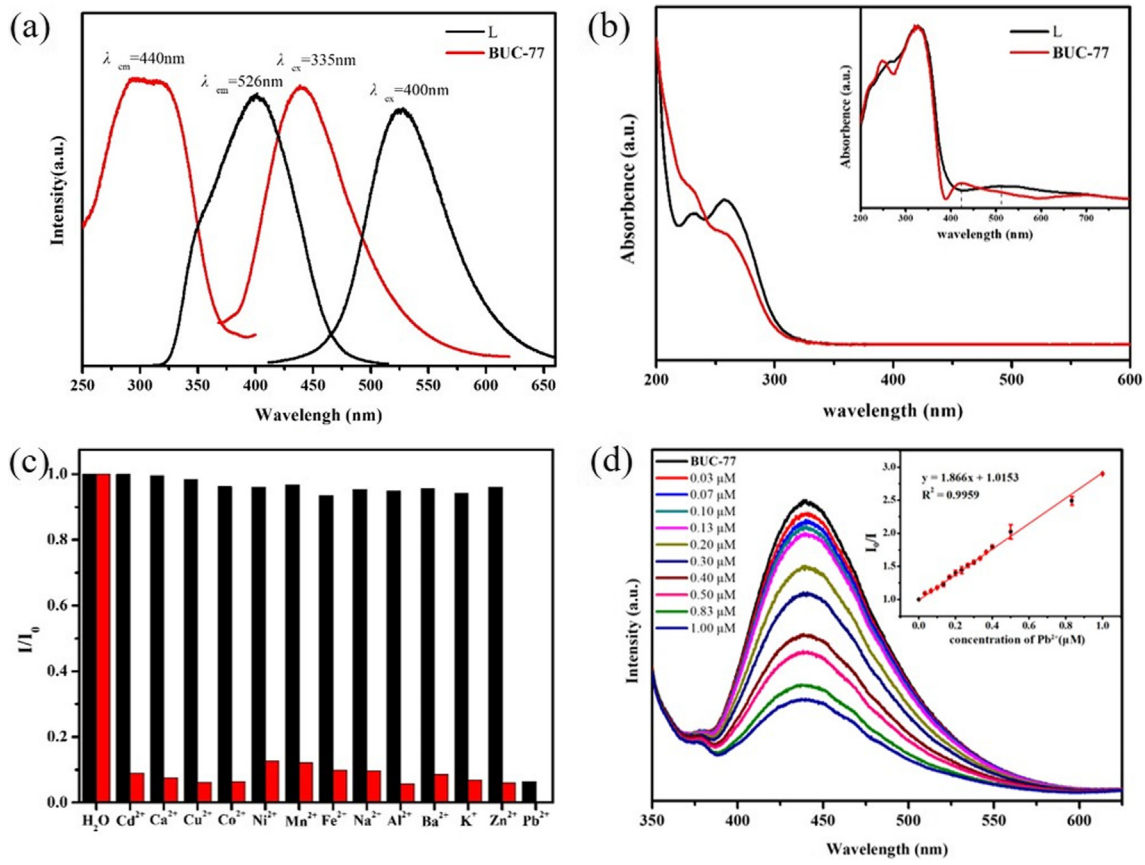

Fig. 2. (a) Excitation and emission spectra and (b) The UV–Vis spectra and DRS UV–Vis spectra (inset) of **BUC-77**. (c) The fluorescence changes of **BUC-77** (1 g/L) upon the addition of various metal cations (10 mM) and $PbCl_2$ (10 mM) in aqueous solution. Left-hand bars represent the fluorescent responses toward metal cations; right-hand bars represent the subsequent addition of $PbCl_2$ to the afore-mentioned solutions. (d) Emission spectra and K_{sv} curve (inset) of **BUC-77** (1 g/L) in aqueous solutions in the presence of various concentrations of Pb^{2+} under excitation at 335 nm.

3.3. Selective sensing detection of Pb^{2+} cations with BUC-77 as fluorescent probe

BUC-77 was stable in aqueous solution at wide pH range from 1.0 to 12.0, which can be affirmed by the PXRD results (Fig. 3a). Also, the strong emissions of **BUC-77** in the solid state make it possible to be used as fluorescent probe to carry out fluorescence detection. As shown in Fig. S2, **BUC-77** demonstrated minor pH-independent fluorescence in the pH range of 1.0–12.0, which indicated that its fluorescence was free of the pH influence.

Considering its good fluorescence and outstanding water stability, **BUC-77** was selected to conduct sensing detection of common metal cations in simulated wastewater. The fluorescent responses of **BUC-77** toward aqueous solutions of various individual metal cations like K^+, Na^+, Mg^{2+}, Ca^{2+}, Cu^{2+}, Zn^{2+}, Co^{2+}, Ni^{2+}, Fe^{2+}, Mn^{2+}, Al^{3+}, Ba^{2+}, Cd^{2+} and Pb^{2+} revealed that only the presence of Pb^{2+} can achieve significant quenching effect (as illustrated in Fig. 2c). In addition, the fluorescence was still quenched when Pb^{2+} and other metal cations were co-existed, implying that **BUC-77** exhibited highly sensitive recognition of Pb^{2+} in the real wastewater.

For better understanding the fluorescent response of **BUC-77** toward Pb^{2+}, the fluorescence titration upon the addition of $PbCl_2$ to **BUC-77** was further conducted. As demonstrated in Fig. 2d, the emission intensity of the **BUC-77** suspension declines sharply

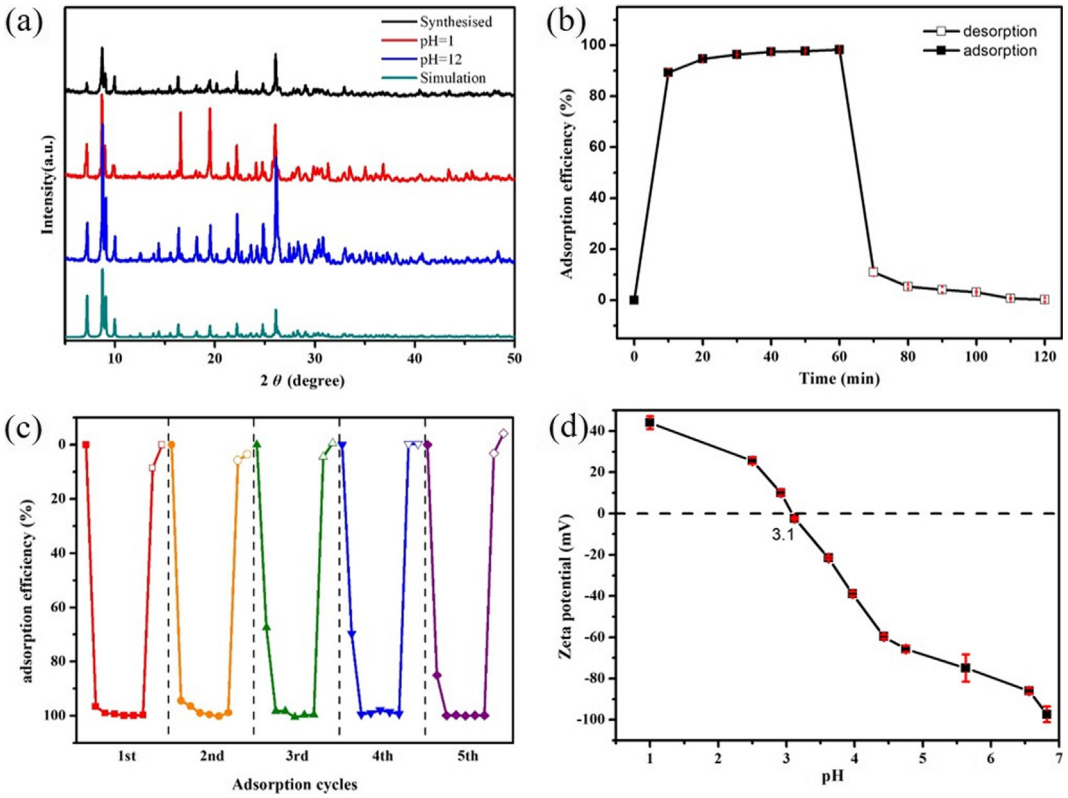

Fig. 3. (a) PXRD patterns of **BUC-77** of as-prepared one, soaked in aqueous for 12 h with pH = 1 and pH = 12 along with the simulated one from single crystal data. (b) The adsorption and desorption efficiency of Pb^{2+}. (c) Cycling adsorption (pH = 3.4) and desorption (pH = 0.92) performances of **BUC-77** toward Pb^{2+} after 60 min adsorption and 20 min desorption. (d) Changes of Zeta potential with pH of **BUC-77**.

with the increase of Pb^{2+} concentration from 0 to 1 μM. This quenching effect can be quantitatively rationalized by the Stern–Volmer equation (1):

$$I_0/I = 1 + K_{sv}[Q] \quad (1)$$

where K_{sv} is the quenching constant, [Q] is the Pb^{2+} concentration, and the values I_0 and I are the fluorescence intensity of the **BUC-77** suspension without and with addition of Pb^{2+}, respectively. As illustrated in Fig. 2d (inset figure), the linear correlation coefficient (R^2) of K_{sv} curve is 0.9959, which suggests that the quenching effect of Pb^{2+} on the fluorescence of **BUC-77** fits the Stern–Volmer model well. The calculated K_{sv} value is 1.866×10^{-3}, indicating a strong quenching effect of Pb^{2+} on the **BUC-77** fluorescence [31,32]. The lowest detectable limit for Pb^{2+} is estimated as 0.03 μM (6.91 ppb), which is below the concentrations of EPA standard limit (15 ppb) [33]. It is speculated that a static quenching process is dominant because the absorption spectrum of **BUC-77** shows obvious difference after contacting with Pb^{2+}. A non-fluorescent complex might be formed between **BUC-77** and Pb^{2+} in the ground state. In the present work, the luminescence quenching effect of POM compound towards metal cations originates from the approach that the cation exchange of central cations in the polyoxomolybdate with targeted cations [34,35]. Thus, it is concluded that **BUC-77** can be potentially utilized to detect Pb^{2+} contamination in the environment with high sensitivity and selectivity.

3.4. Adsorption performance

The adsorption performance of **BUC-77** toward Pb^{2+} was tested with the simulated wastewater containing Pb^{2+}. The corresponding isotherm models, thermodynamic parameters and kinetic studies were omitted in this paper, and only the Pb^{2+} removal efficiency *vs* time and the maximum adsorption capacity were investigated. As illustrated in Fig. 3b, the adsorption efficiency of **BUC-77** toward Pb^{2+} increased rapidly to 89.3% at 10 min, which might be attributed to many available vacant adsorption sites at the beginning, and maintained as plateau at ca. 98% after 30 min. The maximum adsorption capacity of **BUC-77** toward Pb^{2+} were 425 mg/g, which is higher than most of the adsorbents reported previously as listed in Table 1.

3.5. Regeneration and recyclability of BUC-77

Efficient regeneration and recyclability of the adsorbents arose intensive attentions in both lab researches and practical applications. In this work, the used **BUC-77** can be regenerated easily via being washed with 0.2 mol/L HNO_3 aqueous solution, in which 90.1% and 99.1% Pb^{2+} ions were released from **BUC-77** after 5 min and 1 h, respectively, as shown in Fig. 3b, indicating it can be regenerated easily via pH adjustment. As shown in Fig. 3c, **BUC-77** can maintain high adsorption efficiency during 5 runs

Table 1
Comparison of the adsorption capacities of Pb^{2+} onto some typical adsorbents.

Adsorbents	Adsorption capacity ($mg\ g^{-1}$)	References
BUC-14	1105.7	[20]
BUC-77	425	This work
$CoFe_2O_4$-rGO	299.4	[36]
Attapulgite clay@carbon	263.8	[37]
Zinc silicate	210	[38]
Ulmus tree leaves	201.1	[39]
Amino functionalized silica spheres	194.4	[40]
Hydroxyapatite	100.0	[41]

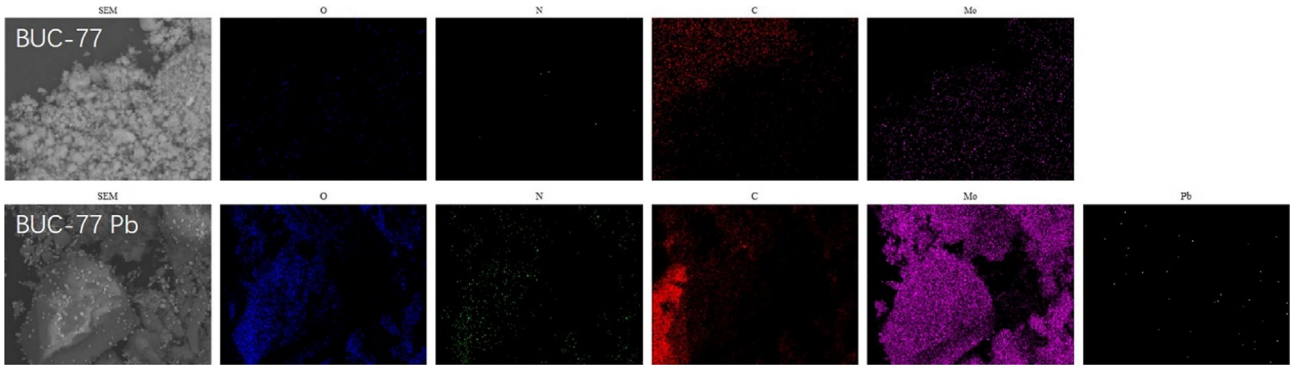

Fig. 4. The C, N, O, Mo and Pb elemental mapping of **BUC-77** before and after adsorption Pb^{2+}.

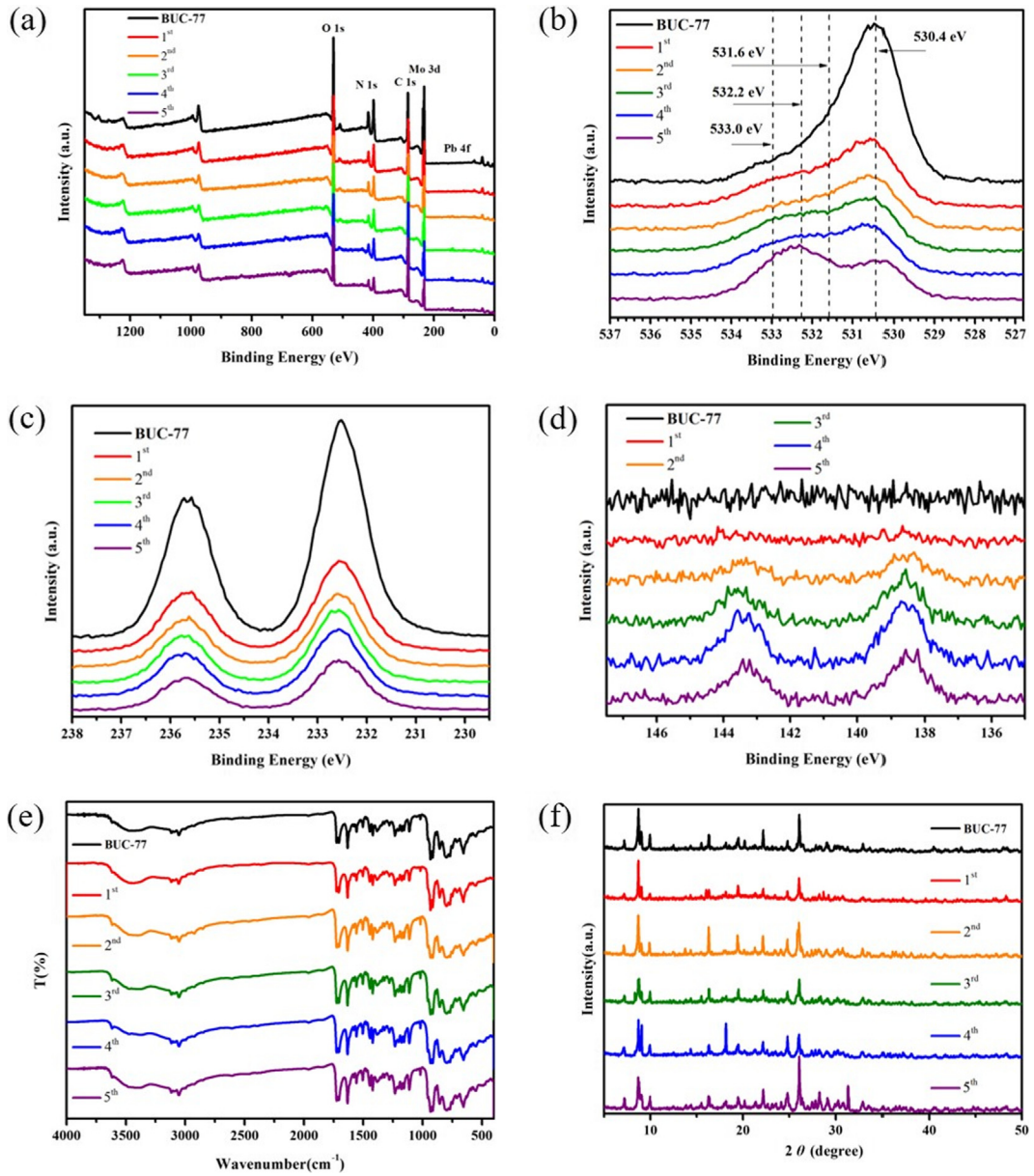

Fig. 5. (a) Full range of XPS spectra, (b) XPS spectra of O 1s, (c) XPS spectra of Mo 3d, (d) XPS spectra of Pb 4f, (e) FTIR spectra and (f) XRD patterns of **BUC-77** before and after the cycle adsorption of Pb^{2+}.

operation, and the slight decrease of adsorption capacity might result from the incomplete desorption of the previous cycles [42].

3.6. Proposed adsorption and desorption mechanisms

Previous studies had illustrated that the surface area was an important factor to influence the adsorption capacity [43,44]. But, in this study, **BUC-77** possessed inferior surface area (1.89 m^2/g) determined by N_2 sorption/desorption measurement, which implied that the strong affinity in binding with Pb^{2+} might not be assigned to its surface area [45]. The surface charge of **BUC-77** was determined via zeta potential measurements in pH range of 2.0–6.0, and the results revealed that the isoelectric point (IEP) values were 3.1, as illustrated in Fig. 3d. The surface charge of **BUC-77** was negative when pH exceeded 3.1 (IEP), indicating that its adsorption activity toward cationic Pb^{2+} can be mainly assigned to the electrostatic interactions [46]. As the pH decreased to 0.7, the surface of **BUC-77** became positively, leading to that the adsorbed Pb^{2+} ions were broken away from the adsorbent [47].

To further clarify the adsorption mechanism, FTIR, PXRD, SEM, and XPS were used to analyze the composition, morphology and microstructure of **BUC-77** before and after adsorption of Pb^{2+}. The elemental mapping obtained from SEM affirmed the presence of Pb^{2+} in **BUC-77** after adsorbing Pb^{2+}, besides C, N, O, and Mo in the as-prepared **BUC-77** (as shown in Fig. 4). As the XPS spectra of O 1s shown in Fig. 5(b), the O 1s region can be decomposed into four peaks at 530.4, 532.2, 531.6 and 533.0 eV, corresponding to Mo—O, O(H_2O), C═O and C—O, respectively. However, the peak attributed to Pb-O bond can't be observed in this study, implying no detectable $PbMoO_4$ was formed in suitable period [48–52]. The XPS spectra as shown in Fig. 5(c) of **BUC-77** revealed that the peaks at 235.58 eV and 232.45 eV were assigned to Mo $3d_{5/2}$ and $3d_{3/2}$ orbitals of Mo^{6+} in the crystal lattice [53,54]. After adsorption of Pb^{2+}, both above-stated doublet peaks were separated by 3.15 eV and the corresponding binding-energy are higher than those in **BUC-77**. Thus, it confirms the existence of the electrostatic interactions between the electron acceptor of Pb^{2+} with the stronger electron-capturing ability and electron-donor of $[Mo_8O_{26}]^{4-}$ [55,56]. The adsorption mechanism was further affirmed by FTIR (Fig. 5e) and PXRD (Fig. 5f), in which there were no obvious differences between the original **BUC-77** and **BUC-77** after adsorbing Pb^{2+}.

4. Conclusions

In this work, guided by a topological design approach, a new chemically stable polyoxomolybdate based hybrid (**BUC-77**) with outstanding fluorescence property has been designed, synthesized, and used to conduct the selective detection and removal of Pb^{2+} ions from water. **BUC-77** exhibited good stability in water and acidic solutions, and demonstrated excellent selective detection ability towards heavy metal Pb^{2+} ions over other partners based on their sensitive fluorescence quenching. The lowest detectable limit of **BUC-77** towards Pb^{2+} is estimated to be 6.91 ppb. As well, **BUC-77** can achieve outstanding adsorption activity toward Pb^{2+} with adsorption capacity up to 425 mg/L, and can be reused just being washed by weak acid aqueous solution. In all, **BUC-77** can achieve "killing two birds with one stone", which provides a new insight into the design of new compounds for the simultaneously detection and removal of contaminates in water.

Acknowledgments

This work was supported by Great Wall Scholars Training Program Project of Beijing Municipality Universities (CIT&TCD20180323), Project of Construction of Innovation Teams and Teacher Career Development for Universities and Colleges Under Beijing Municipality (IDHT20170508), Beijing Talent Project (2017A38), the Fundamental Research Funds for Beijing Universities (X18075/X18076/X18124/X18125/X18276) and Scientific Research Foundation of Beijing University of Civil Engineering and Architecture (KYJJ2017033/KYJJ2017008).

Appendix A. Supplementary material

Crystallographic data, and structure data and thermal properties. CCDC 1850838(BUC-77). CCDC 1850838 contains the supplementary crystallographic data for this paper. These data can be obtained free of charge from the Cambridge Crystallographic Data Centre via www.ccdc.cam.ac.uk/data_request/cif. Supplementary data associated with this article can be found, in the online version, at https://doi.org/10.1016/j.jcis.2018.08.029.

References

[1] C.C. Wang, Y.S. Ho, Scientometrics 109 (2016) 1–33.
[2] Z. Hasan, N.A. Khan, S.H. Jhung, Chem. Eng. J. 284 (2016) 1406–1413.
[3] C.C. Wang, J.R. Li, X.L. Lv, Y.Q. Zhang, G. Guo, Energy Environ. Sci. 7 (2014) 2831–2867.
[4] C.C. Wang, X.D. Du, J. Li, X.X. Guo, P. Wang, J. Zhang, Appl. Catal. B Environ 193 (2016) 198–216.
[5] X.-Y. Xu, C. Chu, H. Fu, X.-D. Du, P. Wang, W. Zheng, C.-C. Wang, Chem. Eng. J. 350 (2018) 436–444.
[6] Y. Peng, Y. Zhang, H. Huang, C. Zhong, Chem. Eng. J. 333 (2018) 678–685.
[7] L. Zhu, D. Sheng, C. Xu, X. Dai, M.A. Silver, J. Li, P. Li, Y. Wang, Y. Wang, L. Chen, J. Am. Chem. Soc. 139 (2017) 14873–14876.
[8] T. Rodenas, I. Luz, G. Prieto, B. Seoane, H. Miro, A. Corma, F. Kapteijn, L.I.X. Fx, J. Gascon, Nat. Mater. 14 (2015) 48–55.
[9] d.V.B. Van, B. Bueken, J. Denayer, V.D. De, Chem. Soc. Rev. 43 (2014) 5766–5788.
[10] B. Chen, S. Xiang, G. Qian, Acc. Chem. Res. 43 (2010) 1115–1124.
[11] A. Liu, C.C. Wang, C.Z. Wang, H.F. Fu, W. Peng, Y.L. Cao, H.Y. Chu, A.F. Du, J. Colloid Interf. Sci. 512 (2017) 730–739.
[12] Y. Guo, X. Feng, T. Han, S. Wang, Z. Lin, Y. Dong, B. Wang, J. Am. Chem. Soc. 136 (2014) 15485–15488.
[13] Z.Q. Shi, Z.J. Guo, H.G. Zheng, Chem. Commun. 51 (2015) 8300–8303.
[14] H. Yamagiwa, S. Sato, T. Fukawa, T. Ikehara, R. Maeda, T. Mihara, M. Kimura, Sci. Rep. 4 (2014) 6247–6253.
[15] X. Zhang, K. Jiang, H. He, D. Yue, D. Zhao, Y. Cui, Y. Yang, G. Qian, Sensor. Actuat. B: Chem 254 (2017) 1069–1077.
[16] Z. Han, Y. Gao, X. Zhai, J. Peng, A. Tian, Y. Zhao, C. Hu, Cryst. Growth Des. 9 (2016) 1225–1234.
[17] H.Y. Zang, Y.Q. Lan, G.S. Yang, X.L. Wang, K.Z. Shao, G.J. Xu, Z.M. Su, CrystEngComm 12 (2010) 434–445.
[18] D.G. Allis, R.S. Rarig, E. Burkholder, J. Zubieta, J. Mol. Struct. 688 (2004) 11–31.
[19] Y.Q. Zhang, C.C. Wang, T. Zhu, P. Wang, S.J. Gao, Rsc Adv. 5 (2015) 45688–45692.
[20] X.D. Du, C.C. Wang, J. Zhong, J.G. Liu, Y.X. Li, P. Wang, J. Environ. Chem. Eng. 5 (2017) 1866–1873.
[21] J.J. Li, C.C. Wang, H.F. Fu, J.R. Cui, P. Xu, J. Guo, J.R. Li, Dalton Trans. 46 (2017) 10197–10201.
[22] D. Hagrman, D.J. ChloeZubieta, J. Rose, R. Zubieta, Haushalter, Angew. Chem. 109 (1997) 904–907.
[23] Z.C. Yue, L.X. Shen, H.H. Wu, X.H. Li, Y.Y. Niu, CrystEngComm 15 (2013) 9938–9948.
[24] Y.Q. Lan, S.L. Li, X.L. Wang, K.Z. Shao, Z.M. Su, E.B. Wang, Inorg. Chem. 47 (2008) 529–534.
[25] Y. P, W. P, X. Z, L. D, B. E, Z. J, C. P, V. DV, L. T, W. Y, Angew. Chem. Int. Ed. 123 (2015) 2569–2573.
[26] Christina A. Bauer, Tatiana V. Timofeeva, Thomas B. Settersten, Brian D. Patterson, Vincent H. Liu, Blake A. Simmons, M.D. Allendorf, J. Am. Chem. Soc. 129 (2007) 7136–7144.
[27] Zhenfeng Chen, J. Rengen Xiong, Xuetai Chen Zhang, A. Ziling Xue, Xiaozeng You, Inorg. Chem. 40 (2001) 4075–4077.
[28] J. Yang, Y. Dai, X. Zhu, Z. Wang, Y. Li, Q. Zhuang, J. Shi, J. Gu, J. Mater. Chem. A 3 (2015) 7445–7452.
[29] X. Gao, H. Zhao, X. Zhao, Z. Li, Z. Gao, Y. Wang, H. Huang, Sensor. Actuat. B: Chem 266 (2018) 323–328.
[30] X.Y. Xu, B. Yan, Sensor. Actuat. B: Chem 230 (2016) 463–469.
[31] N.J.B. Green, S.M. Pimblott, M. Tachiya, J. Phys. Chem. 123 (1993) 97–102.
[32] A. Nitzan, J. Jortner, J. Kommandeur, E. Drent, Chem. Phys. Lett. 9 (1971) 273–278.
[33] L. Beqa, A.K. Singh, S.A. Khan, D. Senapati, S.R. Arumugam, P.C. Ray, A.C.S. Appl, Mater. Interfaces 3 (2011) 668–673.
[34] T. Htun, J. Fluoresc. 14 (2004) 217–222.

[35] J. Keizer, J. Am. Chem. Soc. 105 (1983) 1494–1498.
[36] Y. Zhang, L. Yan, W. Xu, X. Guo, L. Cui, L. Gao, Q. Wei, B. Du, J. Mol. Liq. 191 (2014) 177–182.
[37] L.F. Chen, H.W. Liang, Y. Lu, C.H. Cui, S.H. Yu, Langmuir 27 (2011) 8998–9004.
[38] J. Qu, C.-Y. Cao, Y.-L. Hong, C.-Q. Chen, P.-P. Zhu, W.-G. Song, Z.-Y. Wu, J. Mater. Chem. 22 (2012) 3562–3567.
[39] M.R. Sangi, A. Shahmoradi, J. Zolgharnein, G.H. Azimi, M. Ghorbandoost, J. Hazard. Mater. 155 (2008) 513–522.
[40] A.M. El-Toni, M.A. Habila, M.A. Ibrahim, J.P. Labis, Z.A. Alothman, Chem. Eng. J. 251 (2014) 441–451.
[41] S.D. Jiang, Q.Z. Yao, G.T. Zhou, S.Q. Fu, J. Phys. Chem. C 47 (2012) 4484–4492.
[42] C. Zhu, X. Dong, Z. Chen, R. Naidu, Int. J. Environ. Sci. Technol. 13 (2016) 1257–1268.
[43] D.P. Li, Y.R. Zhang, X.X. Zhao, B.X. Zhao, Chem. Eng. J. 232 (2013) 425–433.
[44] Y. Li, Z. Yang, Y. Wang, Z. Bai, T. Zheng, X. Dai, S. Liu, D. Gui, W. Liu, M. Chen, Nat. Commun. 8 (2017) 1354–1365.
[45] X. Zhao, H. Zhao, W. Dai, Y. Wei, Y. Wang, Y. Zhang, L. Zhi, H. Huang, Z. Gao, J. Colloid Interf. Sci. (2018) 28–34.
[46] X.D. Du, C.C. Wang, J.G. Liu, X.D. Zhao, J. Zhong, Y.X. Li, J. Li, P. Wang, J. Colloid Interf. Sci. 506 (2017) 437–441.
[47] Z.C. Wu, Z.Z. Wang, J. Liu, J.H. Yin, S.P. Kuang, Int. J. Biol. Macromol. 81 (2015) 838–846.
[48] W. Tian, Q. Gao, Y. Tan, K. Yang, L. Zhu, C. Yang, H. Zhang, J. Mater. Chem. *A* 3 (2015) 5656–5664.
[49] Y. Zhang, Y. Su, X. Zhou, C. Dai, A.A. Keller, J. Hazard. Mater. 263 (2013) 685–693.
[50] H. Gu, Y. Guo, S.Y. Wong, C. He, X. Li, V.P.W. Shim, Compos. Sci. Technol. 75 (2013) 62–69.
[51] H.B. Noh, S.B. Revin, Y.B. Shim, Electrochim. Acta 139 (2014) 315–322.
[52] Z. Dai, F. Qin, H. Zhao, F. Tian, Y. Liu, R. Chen, Nanoscale 7 (2015) (1999) 11991–12001.
[53] H. Li, W. Li, S. Gu, F. Wang, H. Zhou, Catal. Sci. Technol. 6 (2015) 3510–3519.
[54] B. Mendoza-Sánchez, T. Brousse, C. Ramirez-Castro, V. Nicolosi, P.S. Grant, Electrochim. Acta 91 (2013) 253–260.
[55] W. Du, L. Liu, K. Zhou, X. Ma, Y. Hao, X. Qian, Appl. Surf. Sci. 328 (2015) 428–435.
[56] M. Zhang, Y. Wang, M. Xu, W. Ma, R. Li, P. Wang, Energy Environ. Sci. 6 (2013) 2944–2949.